J Mater Sci (2011) 46:451–459
DOI 10.1007/s10853-010-4914-5

Effect of Sc, Zr, and Ti on the interfacial reactions of the B_4C/Al system

J. Lai · Z. Zhang · X.-G. Chen

Received: 22 June 2010 / Accepted: 9 September 2010 / Published online: 28 September 2010

Abstract B_4C plates were immersed in liquid aluminum alloyed with Sc, Zr, and Ti to investigate the interfacial reactions between B_4C and liquid aluminum at 730 °C. The influences of alloying elements on the interfacial microstructure and reaction products in terms of individual and combined additions were examined using a scanning electron microscopy (SEM) and a transmission electron microscopy (TEM). Results reveal that all three elements react with B_4C and form interfacial layers that act as a diffusion barrier to limit the decomposition of B_4C in liquid aluminum. The interfacial reactions and the reaction products in each system are outlined. Moreover, by the combined addition of Sc, Zr, and Ti, most of the Ti is enriched at the interface, which not only offers appropriate protection of the B_4C but also reduces the consumption of Sc and Zr at the interface.

Introduction

Particulate reinforced aluminum metal matrix composites (MMCs) are widely used in automotive, aerospace, and nuclear industries because of their improved mechanical, physical, and material properties over conventional monolithic aluminum alloys [1, 2]. As an attractive reinforcement in MMCs [3, 4], boron carbide possesses a series of unique properties, namely low density of 2.51 g/cm^3 that is less than aluminum (2.7 g/cm^3) [5], high impact and wear resistance [6, 7], good resistance to chemical agents [3], and high capacity for neutron absorption [3, 8, 9]. Among other properties, the special capacity of neutron absorption makes Al–B_4C MMCs valuable as neutron shielding materials, which have been increasingly utilized for fabricating the transport and storage containers of spent nuclear fuels in the nuclear industry [10–12]. However, during storage, the spent nuclear fuels introduce a large amount of radionuclides and generate a high heat output [13]. This requires the mechanical properties of the shielding materials to be maintained stable at elevated temperatures for long periods of time.

Al–Sc alloys are attractive matrix materials due to their excellent elevated temperature properties [14–16]. During heat treatment, the hard and coherent Al_3Sc precipitates can be formed from the supersaturated solid solution, which have a $L1_2$ structure and a low coarsening rate at elevated temperatures. Al–Sc binary alloys were reported to exhibit a good softening resistance up to 300 °C [15, 16]. Addition of Zr into Al–Sc alloys can further improve the thermal stability of Al–Sc materials. In combination with Zr, the maximum effect of precipitation strengthening of Al–Sc–Zr ternary alloys can be achieved during annealing in temperatures up to 350 °C [17]. Moreover, the improvement of strength can be maintained much longer than for that of the Al–Sc binary alloys [18]. Therefore, Al–Sc and Al–Sc–Zr alloys are considered to be potential candidates for the matrix materials used for fabricating the Al–B_4C composites that require high thermal stability and good mechanical properties at elevated temperatures.

It is well known that the interface between the reinforcement and the matrix plays an important role in the mechanical properties of the MMCs. During the liquid mixing cast process, Al had poor wettability on B_4C below 1273 K, resulting in poor bonding between the metal and the reinforcement [19–21]. In addition, the strong reactions

J. Lai · Z. Zhang · X.-G. Chen (✉)
Department of Applied Science, University of Québec at Chicoutimi, 555, boulevard de l'Université, Chicoutimi, QC G7H 2B1, Canada
e-mail: xgrant_chen@uqac.ca

between liquid Al and B_4C particles caused the degradation of boron carbide, which reduced the fluidity during casting and deteriorated the mechanical properties [22–24]. It was found that B_4C particles could be easily incorporated into molten aluminum if a Ti-contained flux was used [25, 26]. In the recent development of manufacturing commercial Al–B_4C composites, Ti has been directly introduced into the aluminum matrix to limit the degradation of B_4C and increase the wettability [8, 12]. Results showed that Ti reacted with B_4C to form a Ti-rich interfacial layer around the B_4C surfaces to protect the B_4C particles from the attack of liquid aluminum [12, 23, 24, 27].

Sc, atomic number 21, is the first element in the group III transition metals of the periodic chart. Close to Sc are Ti and Zr, the first and second elements in the group IV transition metals with atomic numbers 22 and 40, respectively. These three alloying elements have some similar behaviors in aluminum alloys. When introducing Sc and Zr into the B_4C/Al system, it is expected that Sc and Zr also react with B_4C to form reaction products and maybe have the beneficial effect of preventing the decomposition of B_4C in the liquid aluminum. On the other hand, such reactions can consume certain amounts of Sc and Zr that are necessary for precipitation strengthening of the Al-matrix. The ultimate properties of Al–B_4C composites depend on the interfacial bonding and the response of the matrix to precipitation hardening. However, the chemical reactivity of Al–Sc and Al–Sc–Zr alloys with B_4C is almost unknown and public information concerning the interfacial reactions in such multi-component systems is very scarce.

In the present study, the effect of Sc, Zr, and Ti on the interfacial reactions and resultant microstructures of B_4C/Al alloys are investigated. The influences of each alloying element are identified by individual addition, while the overall effects of all three elements are studied by a combined addition in the B_4C/Al–Sc–Zr–Ti system. The morphology, element distribution, as well as the reaction-induced phases at the interface for each system have been characterized. This will provide some guidance for the development and manufacture of B_4C particulate reinforced aluminum MMCs.

Experimental

The boron carbide plates used in this study were prepared by hot pressing with 98% of theoretical density, fabricated by Feldco International (Ladera Ranch, CA, USA) under the lot# 255BC. The feedstock powder has an average particle size of 7 μm and a purity of 99.15 wt% B_4C. The chemical composition of B_4C powder, provided by the manufacturer, is listed in Table 1. The plate was cut into a few of rectangular coupons measuring 30 mm long by 3 mm wide by 3 mm thick. All B_4C coupons were degreased in alcohol and ultrasonically cleaned for 5 min.

Table 1 The chemical composition of B_4C powder (wt%)

B_4C			B_2O_3	Fe	O	N	Ca	Si
B	C	Total						
80.44	18.71	99.15	0.196	0.202	0.107	0.115	0.084	0.065

Four aluminum alloys with designed compositions (see Table 2) were made from pure Al (99.99%) and different master alloys, namely Al–2 wt% Sc, Al–15 wt% Zr, and Al–10 wt% Ti. To prepare the experimental alloy bath, approximately 100 g of pure Al was first melted in an alumina crucible. Desired amounts of Sc, Zr, and Ti were then added into the liquid Al in the forms of master alloys. After the molten alloy stabilized at 730 °C, the B_4C coupon was carefully immersed in the alloy bath and was suspended by a fixed unit using the experiment set-up shown in Fig. 1. The molten alloy temperature was maintained at 730 °C for each test. The solid–liquid reaction was stopped after a fixed reaction time t ($t = 2$ and 10 h), following the solidification and cooling of the crucible sample in the air.

The crucible samples (Al plus B_4C bar) were transversely sectioned approximately 10 mm from the top and were metallographically polished using down to 1 μm diamond suspension. The interfacial microstructure and reaction products were analyzed using optical microscopy,

Table 2 Chemical compositions of Al alloys used

No.	Alloying elements (wt%)			Pure Al
	Sc	Zr	Ti	
1	0.30	/	/	Balance
2	/	0.30	/	
3	/	/	0.30	
4	0.30	0.30	0.30	

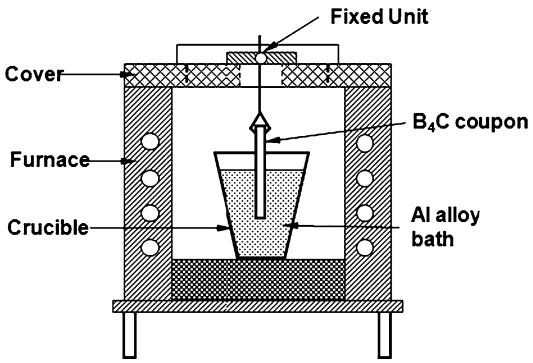

Fig. 1 Schematic diagram of the experiment set-up

scanning electron microscopy (SEM, JEOL JSM-6480LV), and transmission electron microscopy (TEM, JEOL JEM-2100) equipped with an energy dispersive X-ray spectroscopy (EDS). To reveal the morphology of the interface, the sample was deep-etched using a 2.5% HF etchant for 10 min and observed under SEM. To identify the reaction phases in the B_4C/Al interface, a thin-foil TEM specimen from different B_4C/Al alloys was prepared using the focused ion beam (FIB) technique.

Results and discussion

Morphology and type of interfacial layers

Figure 2 shows the morphology of interfacial layers of B_4C/Al alloys with individual or combined additions of alloying elements after a 10-h reaction period. In all the experiments, independent of the reaction time, two distinctive layers are observed at the interface of B_4C with molten aluminum. The lamellar layer close to the surface of boron carbide is composed of fine crystals and the serrated layer on the side of the Al-matrix is made up of coarse facetted crystals with growth orientations toward the aluminum.

It is evident that all four aluminum alloys react with B_4C and form a fine crystal layer following a pile of coarse particles (the coarse crystal layer). After a 2-h reaction period, it was observed that the fine crystal layer already enclosed all the B_4C surfaces and formed a continuous layer in the four alloy systems. Some rough particles randomly grew from the fine crystal layer toward the Al-matrix and formed a discontinuous layer. With the reaction prolonged to 10 h, the thickness of the fine crystal layer increased with different rates in each system. Large particles attached to the fine crystal layer continued to grow and coarsen in the direction of the Al-matrix. Figure 3 illustrates the growth of the interfacial layers with the reaction time in the examples of the B_4C/Al–Ti and B_4C/Al–Zr systems.

In the diffusion perspective, the fine crystal layer can act as a real diffusion barrier in the separation of B_4C from liquid aluminum and, in consequence, the degradation of B_4C was effectively restrained. Therefore, the average thickness of the fine crystal layer for each B_4C/Al system was measured after reacting for 2 and 10 h. Because its thickness was not uniform in the micro scale, the average value was taken from the measurements of SEM images over 50 iterations. Results are plotted in Fig. 4. In the case of adding the alloying element individually, the Al–Sc alloy produced the thickest layer that reached approximately 0.5 μm thick after a 2-h reaction period. The thicknesses of the fine crystal layers were almost equivalent for the Al–Zr and Al–Ti alloys and were about 0.25 μm after holding in the liquid aluminum for 2 h. The values were only half as that in the Al–Sc system. It is interesting to notice that the combined introduction of all alloying elements produced a fine crystal layer whose thickness was almost equal to the values obtained in the Al–Ti and Al–Zr systems.

As the reaction time prolonged to 10 h, the thickness values of the fine crystal layers increased 140%, 90%, and 8% for the Al–Sc, Al–Ti, and Al–Zr systems, respectively, when compared to the values obtained after a 2-h reaction period. The fine crystal layer of the Sc-containing system reached approximately 1.4 μm and was nearly 2.4 times thicker than the Ti-containing system. The Zr-containing system showed the thinnest fine crystal layer and there was almost no increase of the thickness as the reaction time increased from 2 to 10 h. Regarding the combined addition of alloying elements, the thickness of the fine crystal layer increased slowly with a medium value of 24% from a 2 to 10-h holding period, which was less than that of the Ti-containing system.

Interfacial microstructure of B_4C/Al–Sc alloy

Transmission electron microscopy (TEM) was used to investigate the detailed microstructure and reaction components of the B_4C/Al–Sc alloy (Fig. 5). It can be seen from Fig. 5a that the B_4C surface was covered with a layer of polycrystalline with random orientations, as well as the large facetted particles extending from the fine crystal layer. The EDS line scan of Al, B, C, and Sc (Fig. 5b) shows the element distributions across the interface, including the polycrystalline layer and the coarse reaction particle layer. Based on the profiles of the elements, the fine crystal layer can be divided into two sublayers. The first sublayer, adjacent to the surface of B_4C, was enriched with Al, B, and C. The second sublayer, adjacent to the coarse particles, was a Sc-rich lamella containing Sc, Al, B, and C. Moreover, toward the Al-matrix, three elements, i.e., Al, Sc, and C, were detected in the coarse particle.

Selected area electron diffraction (SAED) was used at different locations for identifying the reaction components and phases. In location I, the component in the first sublayer of the fine crystal layer was indexed to be Al_3BC (Fig. 5c). In the second Sc-rich sublayer, the ring patterns from location II are determined to be a mixture of Al_3BC, ScB_2, and Al_3ScC_3 fine crystals (Fig. 5d). In the outside coarse particle layer, two phases were identified using the series sample tilting. In location III, the facetted particles, growing toward the Al-matrix, were identified as Al_3ScC_3 (Fig. 5e, f). The hexagonal particle in location IV, also adjacent to the Al-matrix, was recognized as ScB_2 (Fig. 5g–i). It is clearly apparent that in the B_4C/Al–Sc

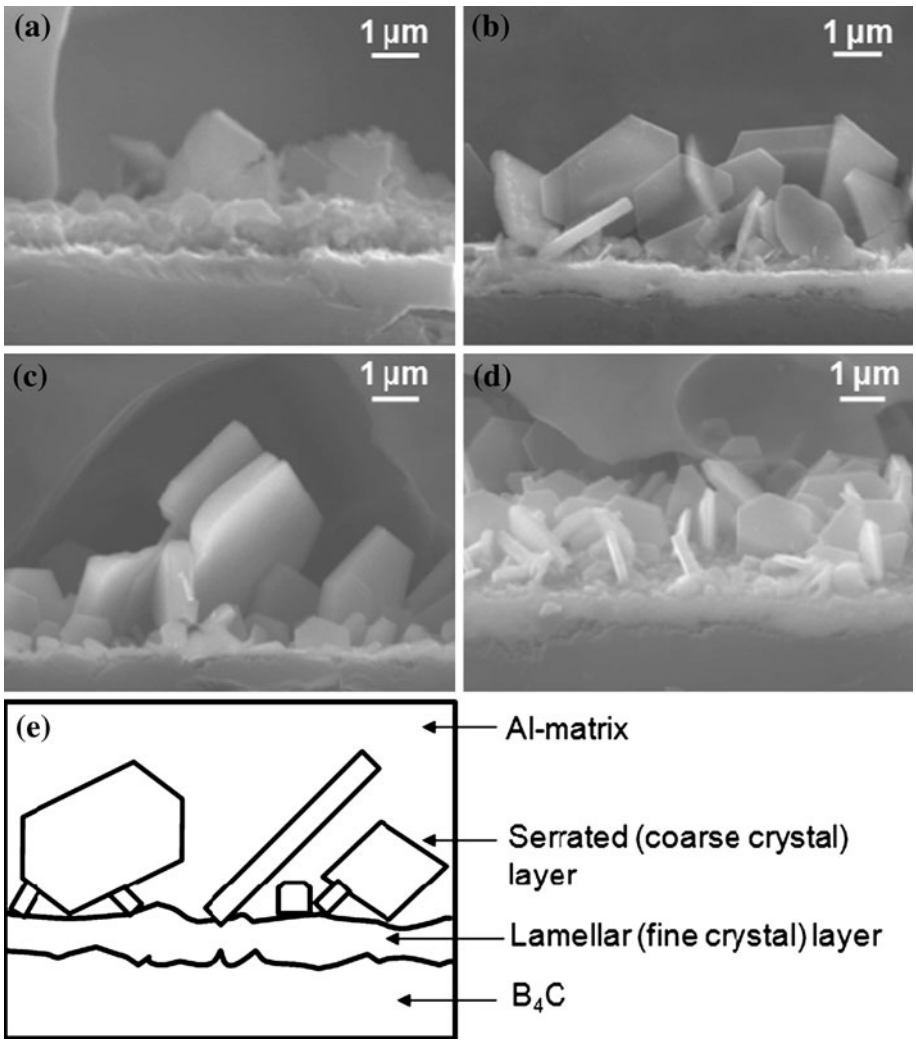

Fig. 2 SEM micrographs of the deep-etched samples revealing the morphology of the interface after 10 h reaction time: **a** B_4C/Al–0.3Sc, **b** B_4C/Al–0.3Ti, **c** B_4C/Al–0.3Zr, and **d** B_4C/Al–0.3Sc–0.3Zr–0.3Ti. **e** Schematic diagram illustrating interfacial layers

system, the fine crystal layer is composed of Al_3BC, ScB_2, and Al_3ScC_3 fine particles, while the coarse layer consists of large Al_3ScC_3 and ScB_2 particles.

Interfacial microstructure of B_4C/Al–Zr alloy

The interface of B_4C/Al–Zr alloy was also studied in detail by TEM, where the B_4C surface was covered with two interfacial layers (Fig. 6a). The annular dark-field STEM image illustrates that two sublayers existed in the fine crystal layer: a dark-gray sublayer close to B_4C is made up of lower Z number elements as well as a white sublayer which enriches higher Z number elements. The coarse crystal layer consists of large plate-like particles which extended from the fine crystal layer toward the Al-matrix.

Results of EDS line scanning indicate that the first sublayer of the fine crystal layer directly attached to B_4C is enriched with Al, B, and C, while the sublayer close to the large particles is concentrated with Zr and B, as shown in Fig. 6b. The SAED ring pattern in location I indicates that the first sublayer consists of Al_3BC crystals (Fig. 6c). The second sublayer in location II is composed of ZrB_2 crystals (Fig. 6d). Large plate-like particles extending into the Al-matrix (location III) are confirmed to be a ZrB_2 phase by the serial sample tilting method (Figs 6e–g). In the literature [28], it was reported that Zr reacted with B_4C to form zirconium diboride (ZrB_2) and zirconium carbide (ZrC). However, in this study, no evidence of zirconium carbide formation was found to be one of the reaction products in the interfacial region.

Interfacial microstructure of B_4C/Al–Ti alloy

For the B_4C/Al–Ti system, it was clearly observed that a fine crystal layer continually covers the surface of B_4C and a number of large particles attach to this layer and grow toward the Al-matrix (Fig. 7a). The EDS line scan from the B_4C to the Al-matrix revealed some Al, B, C in the B_4C side and it changed to mainly Ti and B toward the Al-matrix (Fig. 7b), suggesting the presence of Al_3BC and

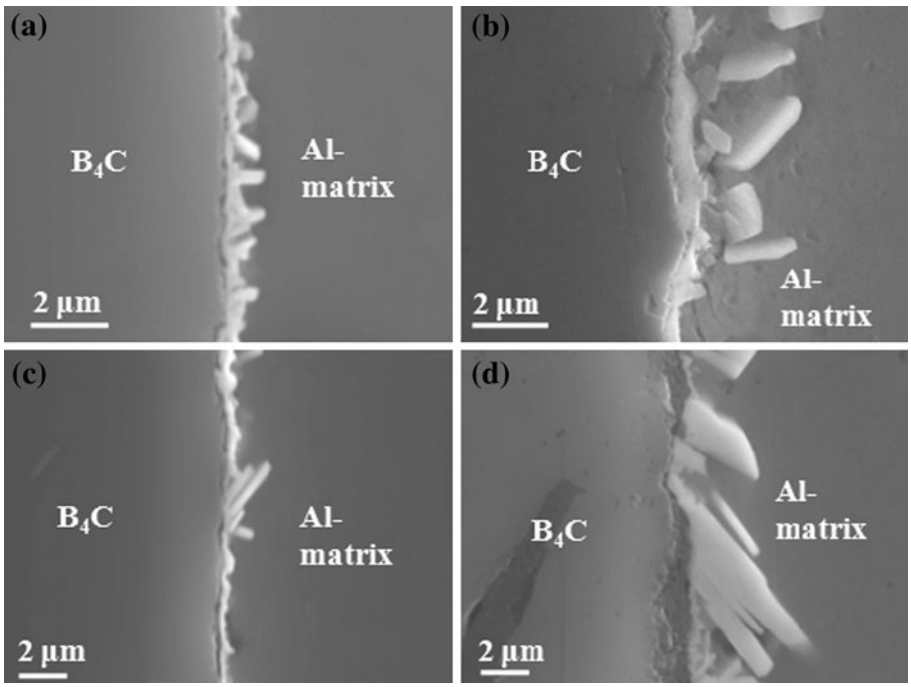

Fig. 3 SEM images showing the interfacial layers at different reaction time: **a** 2 h and **b** 10 h in B_4C/Al–Ti system; **c** 2 h and **d** 10 h in B_4C/Al–Zr system

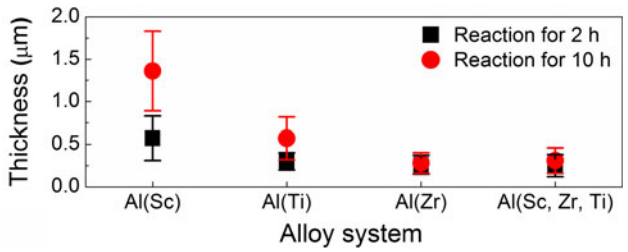

Fig. 4 The thickness evolution of the fine crystal layer in different alloy systems after 2 and 10 h reaction times

TiB_2 compounds in the fine crystal layer as well as TiB_2 particle in the coarse crystal layer. The nature of the interfacial reactions between the B_4C and Al–Ti alloys has been established in recent studies [23, 24, 27]. It was identified by TEM that, while the reaction products close to B_4C were Al_3BC crystals and fine crystals of TiB_2 in the nano scale, the coarse particles near the Al-matrix were identified as TiB_2 phase [23, 24].

Interfacial microstructure of B_4C/Al–Sc–Zr–Ti alloy

In the situation of combined addition of all three alloying elements, the typical microstructure of reaction layers in the interface is shown in Fig. 8a. It can be seen that the B_4C surface is covered with a light-gray sublayer which contains Al, B, and C (Fig. 8b). There is also a dark-gray sublayer which measures approximately 0.1 μm thick and is composed of many tiny crystals on a nanometer scale. Results of the EDS line scan indicate that this sublayer is enriched with Ti, Sc, and B with a small amount of Zr (Fig. 8b). Several coarse reaction particles, ranging from 0.2 to 2 μm, make up the discontinuous coarse layer toward the Al-matrix. This coarse layer is concentrated with Ti and B and contains traces of Sc and Zr. It is interesting to note that a large amount of Ti concentrates at the interfacial layers, while small amounts of Sc and Zr are detectable at the interface.

The SAED ring pattern in area I confirms that the first sublayer close to the B_4C consists of polycrystalline Al_3BC (Fig. 8c). The second sublayer, adjacent to the coarse particles in area II, is composed mainly of TiB_2 type nanocrystals (Fig. 8d), in which Sc and Zr atoms may replace some Ti atoms in the TiB_2 phase. The outside coarse layer near the Al-matrix (area III) consists of large single-crystalline TiB_2 type particles (Fig. 8e–g) which contains a trace amount of Sc and Zr.

Discussion

The microstructural observation reveals that all B_4C/Al systems studied in this work show some common features at the interface. The instability of boron carbide in liquid aluminum triggers the interaction between B_4C and the melt. All three alloying elements react with B_4C and form reaction products and layers covering the B_4C surface. The interfacial region consists of two distinctive layers: a fine crystal layer close to the B_4C and a coarse crystal layer near the Al-matrix. During immersion testing, the B_4C plate contacts with the liquid and aluminum and alloying elements react with B_4C. This leads to the dissolving and the release of B and C atoms into molten aluminum. Since

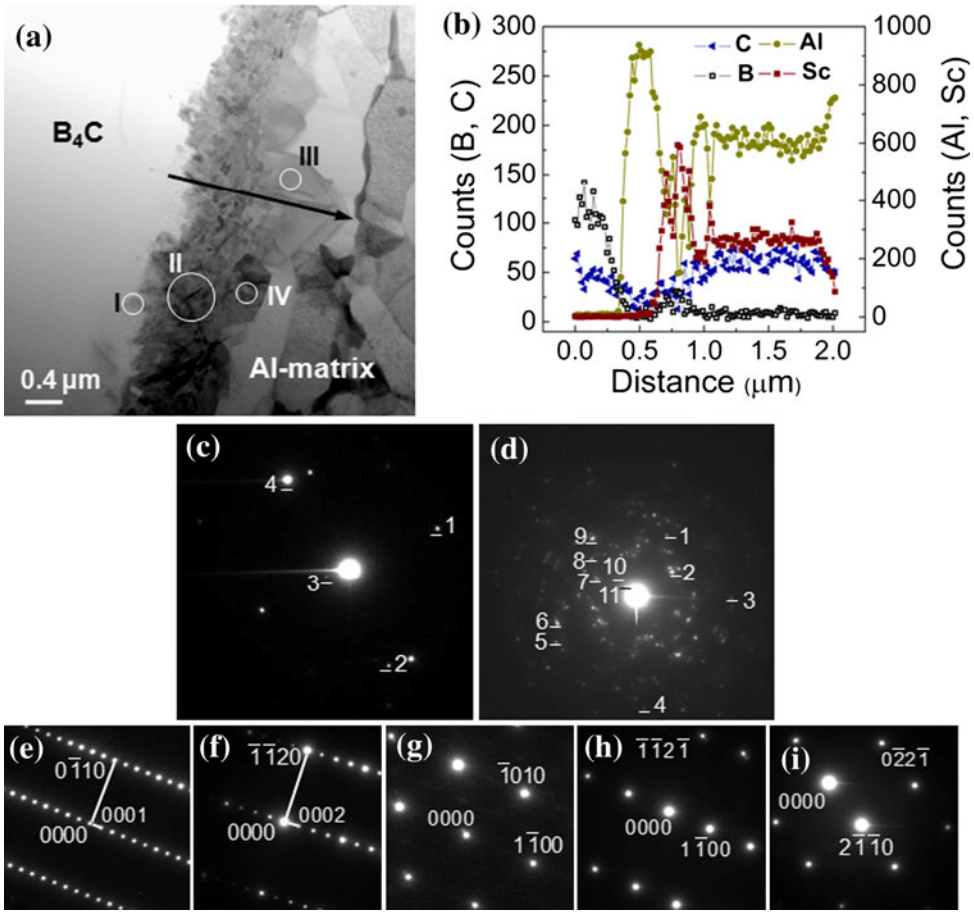

Fig. 5 **a** Bright-field STEM image of interfacial layers in Sc-containing Al–B_4C couple, **b** EDS line scan of Al, Sc, B, and C along the *arrow* in **a**, **c** SAED ring pattern from selected area I: *1* Al_3BC (101), *2* Al_3BC (102), *3* Al_3BC (001), *4* B_4C (104). **d** SAED ring pattern from selected area II: *1* ScB_2 (110), *2* ScB_2 (100), *3* ScB_2 (201), *4* ScB_2 (211), *5* Al_3BC (116), *6* Al_3BC (203), *7* Al_3BC (101), *8* Al_3BC (104), *9* Al_3BC (112), *10* Al_3ScC_3 (004), *11* Al_3ScC_3 (002). **e**, **f** Al_3ScC_3 phase electron diffraction patterns corresponding to the selected area III at the respective zone axes $[2\bar{1}\bar{1}0]$ and $[1\bar{1}00]$. **g–i** ScB_2 phase electron diffraction patterns from the selected area IV at the respective zone axes $[000\bar{1}]$, $[11\bar{2}\bar{6}]$, and $[01\bar{1}\bar{4}]$

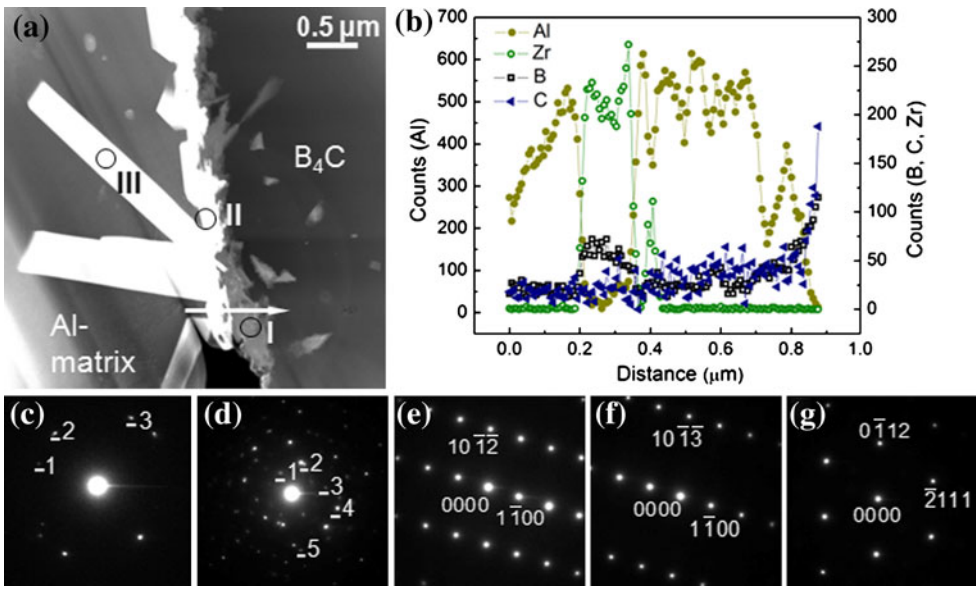

Fig. 6 **a** Dark-field STEM image of interfacial layers in Zr-containing Al–B_4C couple, **b** EDS line scan of Al, B, C, Zr along the *arrow* indicated in **a**. **c** SAED ring pattern from region I: showing polycrystalline Al_3BC: *1* (101), *2* (102), 3 (103). **d** SAED ring pattern from region II: *1* Al (200), *2* ZrB_2 (102), *3* ZrB_2 (200), *4* ZrB_2 (211), *5* ZrB_2 (104). **e–g** ZrB_2 electron diffraction patterns corresponding to the selected area III at the respective zone axes of $[22\bar{4}3]$, $[11\bar{2}1]$, and $[25\bar{7}6]$

the solubility of boron and carbon in aluminum is low (~1000 ppm for boron at 1000 K [22] and 6 ppm for carbon even at 1223 K [29]), carbides and borides precipitate from the saturated liquid as reaction products. The fine reaction crystals form at the surface of the B_4C. As the number of fine crystals continues to increase with increased reaction time, it builds up the first interfacial layer that progressively encloses all the B_4C surfaces. When prolonging the reaction time, the reaction particles begin to grow and coarsen toward the liquid aluminum.

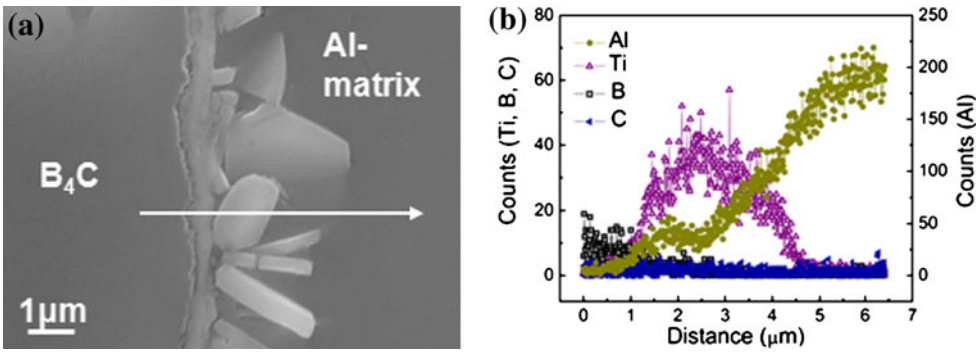

Fig. 7 **a** SEM image of interfacial layer of B_4C/Al-Ti couple. **b** EDS line profiles showing major element distributions along the *white arrow* in **a**

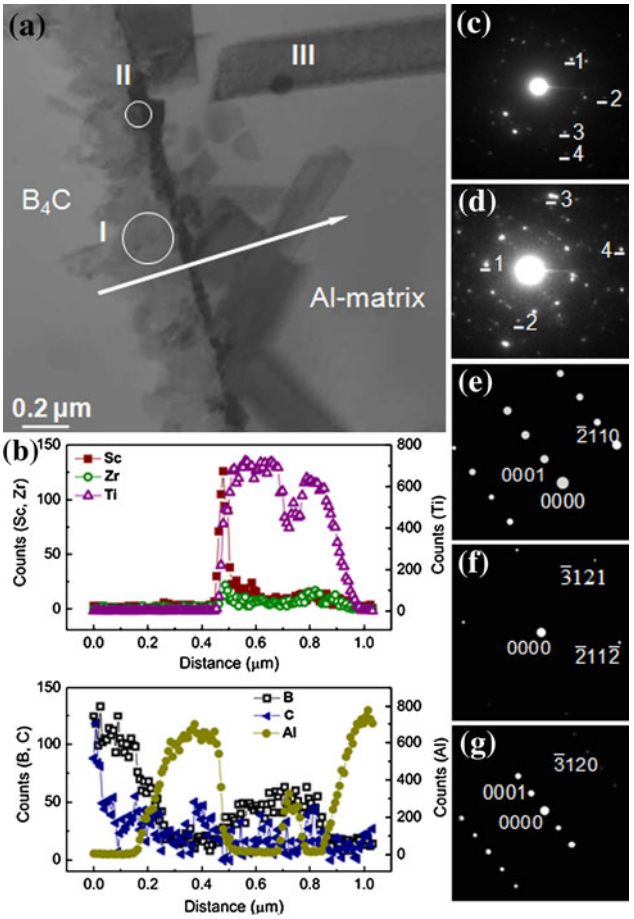

Fig. 8 **a** Bright-field STEM image of interfacial layers in Sc, Zr, and Ti containing Al–B_4C couple, **b** EDS line scan of Al, B, C, Sc, Zr, and Ti along the *arrow* indicated in **a**. **c** SAED ring pattern from region I showing polycrystalline Al_3BC: *1* (101), *2* (105), *3* (103), *4* (110). **d** SAED ring pattern from region II showing polycrystalline Al_3BC and TiB_2: *1* TiB_2 (101), *2* Al_3BC (110), *3* TiB_2 (201), *4* Al_3BC (201). **e**–**g** TiB_2 electron diffraction patterns corresponding to the selected area III at the respective zone axes of $[01\bar{1}0]$, $[\bar{2}13\bar{1}3]$, and $[\bar{1}5\bar{4}0]$

In the binary B_4C/Al system, reaction between B_4C and liquid aluminum takes place according to the following interfacial reaction [22, 23]:

$$9Al + 2B_4C = 2Al_3BC + 3AlB_2 \quad (1)$$

Two reaction products, Al_3BC and AlB_2, form at the interface. In our preliminary tests, the interfacial reaction between pure liquid aluminum and B_4C plate was also studied in the immersion testing. Results showed that the formation of Al_3BC and AlB_2 at the interface led to a quick decomposition of B_4C, which confirmed the fact that these two compounds are unable to prevent the attack of liquid aluminum on B_4C [22–24, 27]. With the addition of alloying elements, the interfacial layers formed at the B_4C surface can act as a diffusion barrier to limit the decomposition of B_4C. For the diffusion perspective, the fine crystal layer is dense and continuous and therefore, it becomes a real barrier in avoiding the direct contact of B_4C with liquid aluminum, which transforms a fast liquid diffusion-controlled process into a slow solid diffusion-controlled process. On the other hand, the coarse crystal layer is less dense and of a discontinuous nature and in consequence, it is less effective in separating B_4C from liquid aluminum. Due to a high affinity with boron and carbon, all three alloying elements have some similar behaviors in the B_4C/Al system, showing that they are concentrated and consumed at the B_4C/Al interface to form reaction products and layers.

Recent research in the Al–B_4C composites revealed that, with the Ti addition in the B_4C/Al alloy, the following interfacial reaction replaces the reaction (1) [23, 24, 27]:

$$6Al + 3Ti + 2B_4C = 2Al_3BC + 3TiB_2 \quad (2)$$

The reaction products, Al_3BC and TiB_2, build a protective layer surrounding the B_4C surface. In the B_4C/Al–Zr alloy, it is found that the fine crystal layer consists of Al_3BC and ZrB_2, while the coarse layer is mainly made of ZrB_2 particles. Similar to the B_4C/Al–Ti system, the interfacial reaction in the B_4C/Al–Zr alloy can be formulated as follows:

$$6Al + 3Zr + 2B_4C = 2Al_3BC + 3ZrB_2 \quad (3)$$

In the B_4C/Al–Sc system, it is identified for the first time that three reaction products exist in the interfacial

microstructure, namely Al_3BC, ScB_2,and Al_3ScC_3. The equation for the interfacial reaction of this system can be expressed as:

$$9Al + 10Sc + 5B_4C = 2Al_3BC + Al_3ScC_3 + 9ScB_2 \quad (4)$$

Taking into account the combined addition of all three alloying elements, mainly two reaction products (Al_3BC and TiB_2 type crystals) in the B_4C/Al–Sc–Zr–Ti system are identified in the fine crystal layer, although some Sc and Zr are also detected in this layer. The outside coarse crystal layer is confirmed to be in the majority of TiB_2 type crystals that also contain traces of Sc and Zr. Due to the fact that most of the Ti but only a small amount of the Sc and Zr concentrate at the interfacial reaction layers, it is reasonable to believe that the interfacial reaction in the B_4C/Al–Sc–Zr–Ti alloy is dominated by reaction (2).

It is worth pointing out that all above mentioned interfacial reactions and its reaction phases took place in the liquid stage. During the immersion tests, after the B_4C plate contacted with liquid aluminum for several hours (2–10 h) at 730 °C, the crucible sample was cooled and solidified in the air. The freeze time of the sample was a few of minutes, which was too short to form the reaction products during solidification. It is reasonable to believe that all reaction phases that were identified by SEM/TEM were formed during liquid holding.

It is observed that the thickness of the fine crystal layer varies for different alloying elements. The B_4C/Al–Sc alloy yields the thickest layer after 2- and 10-h reaction periods. According to the TEM result (Fig. 5), the ring patterns of the fine crystal layer are made up of discrete spots suggesting relatively large-size crystals of reaction products collected at the interface. Large grains pile up at the interface as a barrier layer, making it less effective to restrain the diffusion of boron and carbide out of the B_4C. As a result, and although a large amount of Sc is consumed at the interface, it is still inefficient to prevent B_4C decomposition. The B_4C/Al–Ti alloy shows a medium thickness of the fine crystal layer after 10 h of holding. It has been demonstrated that a Ti-rich layer forms at the B_4C interface and its reaction product TiB_2 is an efficient barrier to limit B_4C decomposition [8, 12, 23, 24, 27]. The ring patterns of the TiB_2 layer obtained in the B_4C/Al–Ti system show many continuous rings, which is recognized as the finest TiB_2 crystals on the nanometer scale [24]. On the other hand, the B_4C/Al–Zr alloy possesses the thinnest layer among the three individual alloying additions, which may suggest that Zr is a potential candidate for stabilizing B_4C during the manufacturing process of Al–B_4C composites.

When introducing all three additives into the B_4C/Al system, the thickness of the fine crystal layer after 10 h of holding is very moderate and lies between the B_4C/Al–Ti and B_4C/Al–Zr alloys. TEM results show that most of the Ti is concentrated at the interface and the layer is composed mainly of a number of TiB_2 type nano-crystals. It is evident that, when co-existing with Sc and Zr, Ti not only offers appropriate protection of the B_4C but also greatly reduces the consumption of Sc and Zr at the interface.

The Al–Sc alloy exhibits particular promise for developing a thermally stable matrix due to the forming of fine and coherent Al_3Sc precipitates upon aging. The addition of the slow diffusing element Zr, which is soluble in Al_3Sc, has the potential to increase the coarsening resistance of Al_3Sc precipitates and thus improve the thermal stability of the matrix during prolonged exposure at elevated temperatures [30, 31]. Moreover, it is reported that Ti is also a candidate as a ternary alloying element to the Al–Sc alloy for stabilizing the precipitate structure and improving the coarsening resistance [31]. Considering the commercial benefits, Sc and Zr, in the form of aluminum master alloys, are more expensive than Ti. Therefore, it is desirable for the thermally stable Al–B_4C composites that Ti be primarily used at the interface to prevent B_4C degradation while most of the Sc and Zr remain in the Al-matrix for precipitation strengthening.

By individual addition of three alloying elements in the B_4C/Al system, the alloying element is enriched at the B_4C/Al interface and bonded in the reaction products, which leaves too little to contribute to the precipitation strengthening. In the case of the combined addition of Sc, Zr, and Ti, most of the Ti is enriched at the interface to build up protective layers around the B_4C and the concentration of Sc and Zr at the interface decreases greatly. Results obtained in this study give an interesting promise that satisfies two important aspects of producing thermally stable Al–B_4C composites, namely the protection of the B_4C and the response of the matrix to precipitation strengthening.

Conclusions

The influences of alloying elements Sc, Zr, and Ti on the interfacial reactions of the B_4C/Al system have been studied in terms of individual and combined additions using the immersion tests. All three alloying elements react with B_4C in liquid Al and form interfacial layers covering the B_4C surface. The interfacial region constitutes two distinctive layers: a fine crystal layer close to the B_4C and the coarse crystal layer near the Al-matrix. For the diffusion perspective, the fine crystal layer is a real barrier in avoiding the direct contact of B_4C with liquid aluminum. The thickness of the fine crystal layer varies with different alloying elements and reaction times.

Three phases of Al_3BC, Al_3ScC_3, and ScB_2 are identified as reaction products in the B_4C/Al–Sc system. Al_3BC

and ZrB_2 in the B_4C/Al–Zr system, as well as Al_3BC and TiB_2 in the B_4C/Al–Ti and B_4C/Al–Sc–Zr–Ti systems are, respectively, confirmed. The interfacial reactions and the reaction products in each system are outlined.

By individual addition of three alloying elements in the B_4C/Al system, the alloying element is mainly enriched at the B_4C/Al interface and bonded in the reaction products. In the case of a combined addition of Sc, Zr, and Ti, most of the Ti is enriched at the interface, which not only offers appropriate protection to the B_4C but also reduces the consumption of Sc and Zr at the interface.

Acknowledgements The authors would like to acknowledge the Natural Sciences and Engineering Research Council of Canada (NSERC) and Rio Tinto Alcan for the financial support through the NSERC Industrial Research Chair in Metallurgy of Aluminium Transformation at the University of Québec at Chicoutimi.

References

1. Surappa MK (2003) Sadhana Acad Proc Eng Sci 28:319
2. Smagorinski ME, Tsantrizos PG, Grenier S, Brzezinski T, Kim G (1998) Mater Sci Eng A 244:86
3. Thevenot F (1990) J Eur Ceram Soc 6:205
4. Ye JC, He JH, Schoenung JM (2006) Metall Mater Trans A 37:3099
5. Lillo TM (2005) Mater Sci Eng A 410:443
6. Bond GM, Inal OT (1995) Compos Eng 5:9
7. Hemanth J (2005) Wear 258:1732
8. Chen XG (2005) In: Schlesinger ME (ed) EPD congress 2005, p 101
9. Gericke MT, Bowman JD, Carlini RD, Chupp TE, Coulter KP, Dabaghyan M et al (2005) J Res Natl Inst Stand Technol 110:215
10. Chen XG, Hark R (2008) In: Yin W, Das SK (eds) Proceedings of aluminum alloys: fabrication, characterization and applications. TMS Annual Meeting, New Orleans, p 3
11. Bonnet G, Rohr V, Chen XG, Bernier JL, Chiocca R, Issard H (2009) Packag Transp Storage Secur Radioact Mater 20:98
12. Chen XG (2006) In: Gupta N, Hunt WH (eds) Proceedings of solidification process of metal matrix composites. TMS Annual Meeting, San Antonio, p 343
13. Yamazaki T, Sanada K, Nishiyama T, Ishii H (2007) In: Proceedings of 15th international symposium on the packaging and transportation of radioactive materials (PATRAM), Miami, Paper # 228
14. Blake N, Hopkins MA (1985) J Mater Sci 20:2861. doi: 10.1007/BF00553049
15. Zakharov VV (2003) Met Sci Heat Treat 45:246
16. Royset J, Ryum N, Bettella D, Tocco A, Jia ZH, Solberg JK, Reiso O (2008) Mater Sci Eng A 483–484:175
17. Fuller CB, Seidman DN, Dunand DC (2003) Acta Mater 51:4803
18. Davydov VG, Elagin VI, Zakharov VV, Rostova TD (1996) Met Sci Heat Treat 38:347
19. Halverson DC, Pyzik AJ, Aksay IA, Snowden WE (1989) J Am Ceram Soc 72:775
20. Suresh S, Mortensen A, Needleman A (1993) Fundamentals of metal-matrix composites. Butterworth-Heinemann, Boston, p 42
21. Delannay F, Froyen L, Deruyttere A (1987) J Mater Sci 22:1. doi: 10.1007/BF01160545
22. Viala JC, Bouix J, Gonzalez G, Esnouf C (1997) J Mater Sci 32:4559. doi:10.1023/A:1018625402103
23. Zhang Z, Chen XG, Charette A (2009) J Mater Sci 44:492. doi: 10.1007/s10853-008-3097-9
24. Zhang Z, Chen XG, Charette A (2007) J Mater Sci 42:7354. doi: 10.1007/s10853-007-1554-5
25. Kennedy AR, Brampton B (2001) Scripta Mater 44:1077
26. Kennedy AR (2002) J Mater Sci 37:317. doi:10.1023/A:1013600328599
27. Zhang Z, Fortin K, Charette A, Chen XG (2010) J Mater Sci (submitted)
28. Zhang GJ, Ando M, Yang JF, Ohji T, Kanzak S (2004) J Eur Ceram Soc 24:171
29. Simensen CJ (1989) Metall Trans A 20:191
30. Fuller CB, Murray JL, Seidman DN (2005) Acta Mater 53:5401
31. van Dalen ME, Seidman DN, Dunand DC (2008) Acta Mater 56:4369